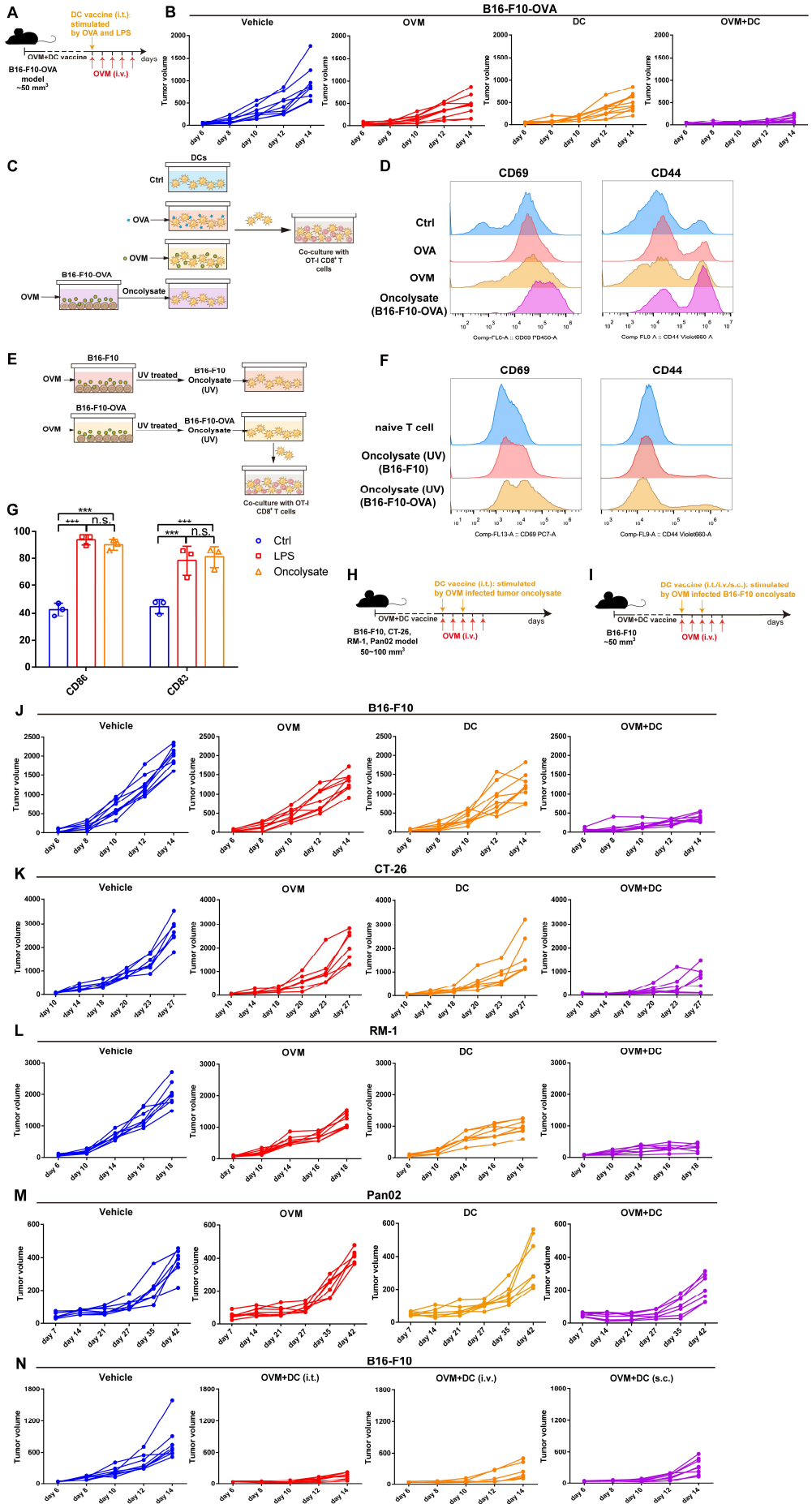


**Cell Reports Medicine, Volume 4**

**Supplemental information**

**Oncolytic virus M1 functions as a bifunctional  
checkpoint inhibitor to enhance  
the antitumor activity of DC vaccine**

**Jia Dan, Jing Cai, Yingqian Zhong, Chaoqun Wang, Shanyu Huang, Ying Zeng, Zhen Fan, Cuiying Xu, Linyi Hu, Jiayu Zhang, Jun Hu, Ying Liu, Xingwen Su, Wenbo Zhu, Guangmei Yan, Jiankai Liang, and Yuan Lin**



**Figure S1. OVM infection releases tumor-associated antigens and enhances the efficacy of DC vaccines in various tumor models, related to Figure 1.**

A-B.) Schematic diagram (A) and tumor growth curves for each mouse (B) in the experimental results shown in Figure 1A.

C-D.) Diagrammatic sketch (C) and the representative histogram of CD69 and CD44 (D) in Figure 1B.

E-F.) Diagrammatic sketch (E) and the representative histogram of CD69 and CD44 (F) in Figure 1C.

G.) The expressions changes of CD86 and CD83 on the CD11c<sup>+</sup> DCs stimulated with vehicle (Ctrl), LPS (500 ng/mL) or B16-F10-derived oncolysate (1 mL) for 24 h. n=3.

H-I.) Schematic diagram of Figure 1D-G (B) and Figure 1H (C).

J-N.) Tumor growth curves for each mouse in the experimental results shown in Figure D-H, respectively.

one-way ANOVA was used to determine the significance of differences between groups.

All data are presented as the means  $\pm$  SDs.

*n.s.*, not significant; \* $p < 0.05$ ; \*\*  $p < 0.01$ ; \*\*\*  $p < 0.001$ .

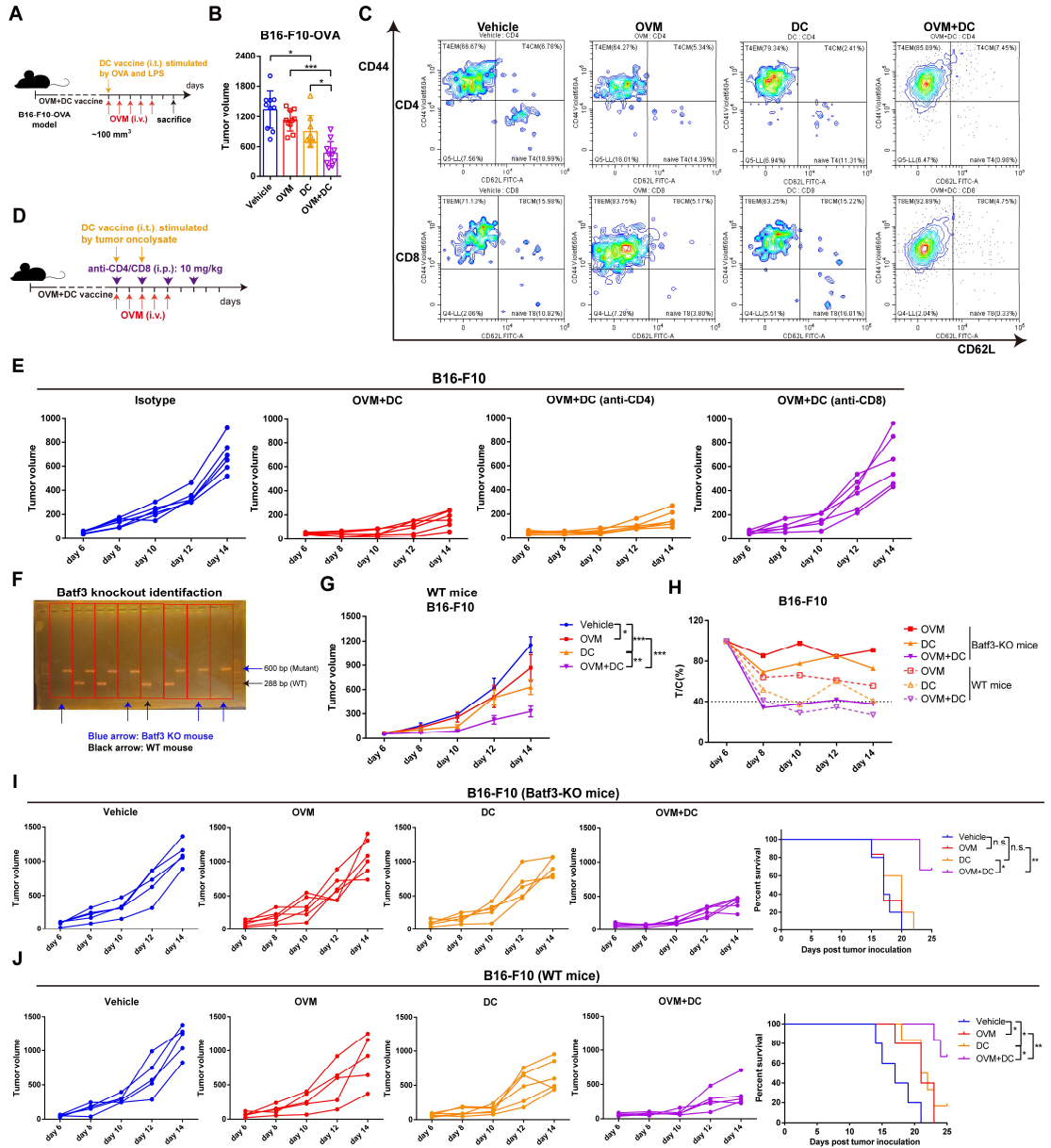


**Figure S2. Combination of OVM and DC vaccine strongly enhances systemic antitumor response, and this efficacy remains unaffected by cDC1s, related to Figure 2.**

A.) Schematic diagram of Figure 2A-R.

B.) The tumor volumes on the second day after the last administration. n=9. Data are presented as the means ± SDs.

C.) Representative plot for the proportion of CD4<sup>+</sup> CD62L<sup>+</sup> T<sub>CM</sub> cells and CD4<sup>+</sup> CD62L<sup>-</sup> T<sub>EM</sub> cells among CD4<sup>+</sup> and CD8<sup>+</sup> T cells, respectively.

D-E.) Schematic diagram of the treatment regimen (D) and tumor growth curves for each mouse (E) in Figure 2S.

F.) Genotype identification of Batf3-KO mice.

G-J.) Batf3-KO mice and their WT littermates were implanted subcutaneously in the right flank with B16-F10 cells on day 0 and received corresponding treatments on day 7. WT mice: n=5 in vehicle and OVM treated group. n=6 in DC vaccine group and n=7 in OVM plus DC vaccine group.

G.) Tumor growth curves of WT mice. *p* values were determined by one-way ANOVA at the final time point as indicated in the graphs.

H.) The T/C% values showing the relative tumor growth rate in every group compared with the vehicle group in Batf3-KO and WT mice.

I-J.) Tumor growth curves for each mouse and Kaplan–Meier survival curves in the Figure 2T (I) and Figure S2G (J), respectively. *p* values were determined by the log-rank test.

*n.s.*, not significant; \**p* < 0.05; \*\**p* < 0.01; \*\*\**p* < 0.001.

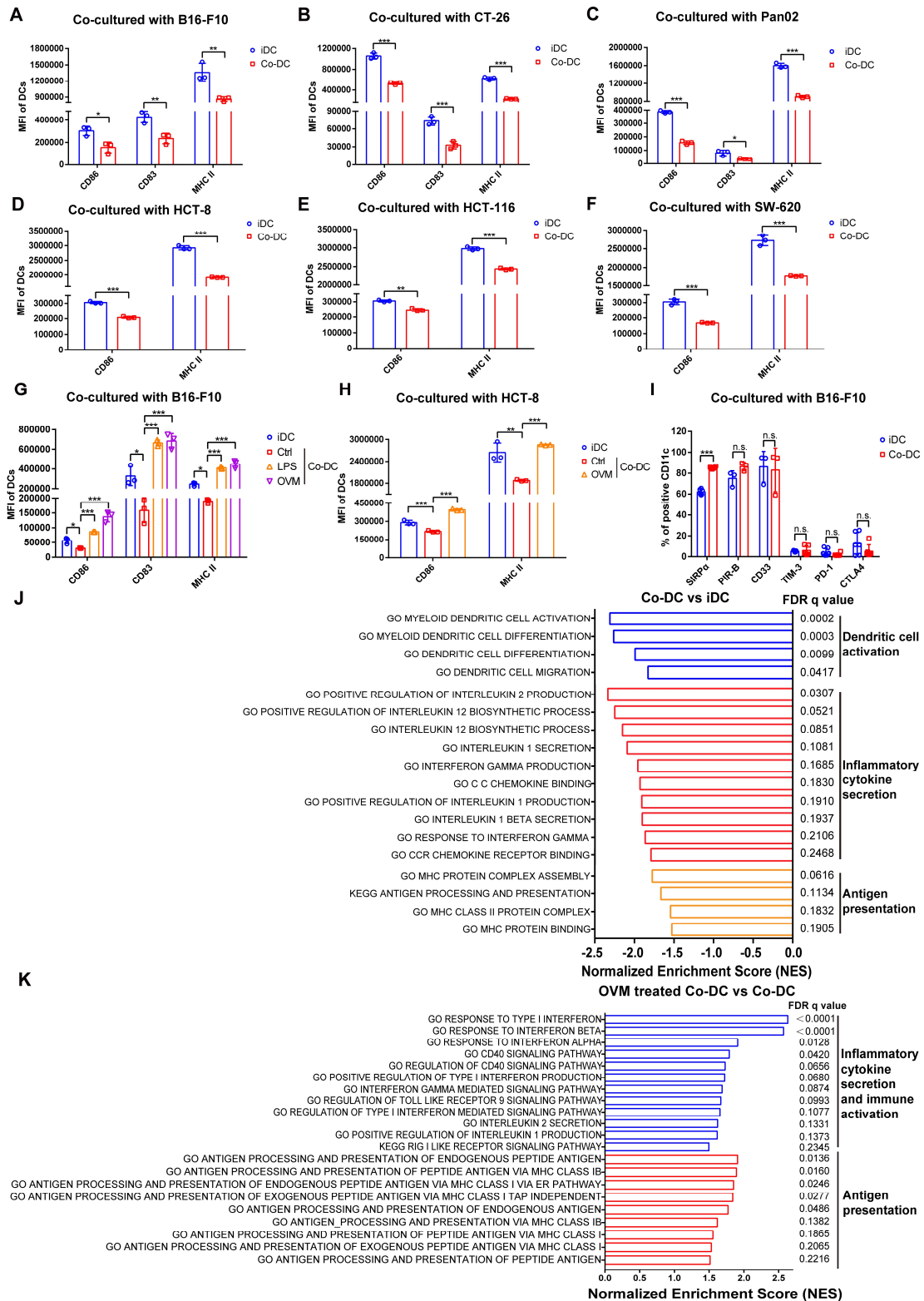


**Figure S3. OVM reactivates the function of DCs inhibited by tumor cells, related to Figure 3.**

A-C.) The MFI of CD86, CD83 and MHC II in mouse CD11c<sup>+</sup> DCs after cocultured at a 3:1 ratio with B16-F10 cells (A), CT-26 cells (B) for 48 h or with Pan02 cells for 72 h (C).

D-F.) The expression of CD86 and MHC II in human CD11c<sup>+</sup> DCs after cocultured at a 3:1 ratio with HCT-8 cells (D), HCT-116 cells (E) or SW-620 cells for 24 h (F).

G.) The MFI changes of CD86, CD83 and MHC II on mouse CD11c<sup>+</sup> DCs cocultured with B16-F10 cells for 24 h and stimulated with control (Ctrl), LPS (1 µg/ml, as a positive control) or OVM (1 MOI) for another 24 h.

H.) The expressions changes of CD86 and MHC II on human DCs cocultured with HCT-8 cells for 24 h and stimulated with vehicle (Ctrl) or OVM (1 MOI) for another 24 h.

I.) The ratio changes of checkpoints on DCs after cocultured with B16-F10 for 48 h.

n=3 in every group. All data are presented as the means ± SDs. *n.s.*, not significant; \**p* < 0.05; \*\**p* < 0.01; \*\*\**p* < 0.001.

J.) GSEA pathways enriched with downregulated genes in cocultured DCs (co-DCs) compared to untreated BMDCs (iDCs).

K.) Pathways enriched with upregulated genes in OVM-treated Co-DCs compared to Co-DCs. *p* < 0.05 and false discovery rate q value (FDR-q) < 0.25.

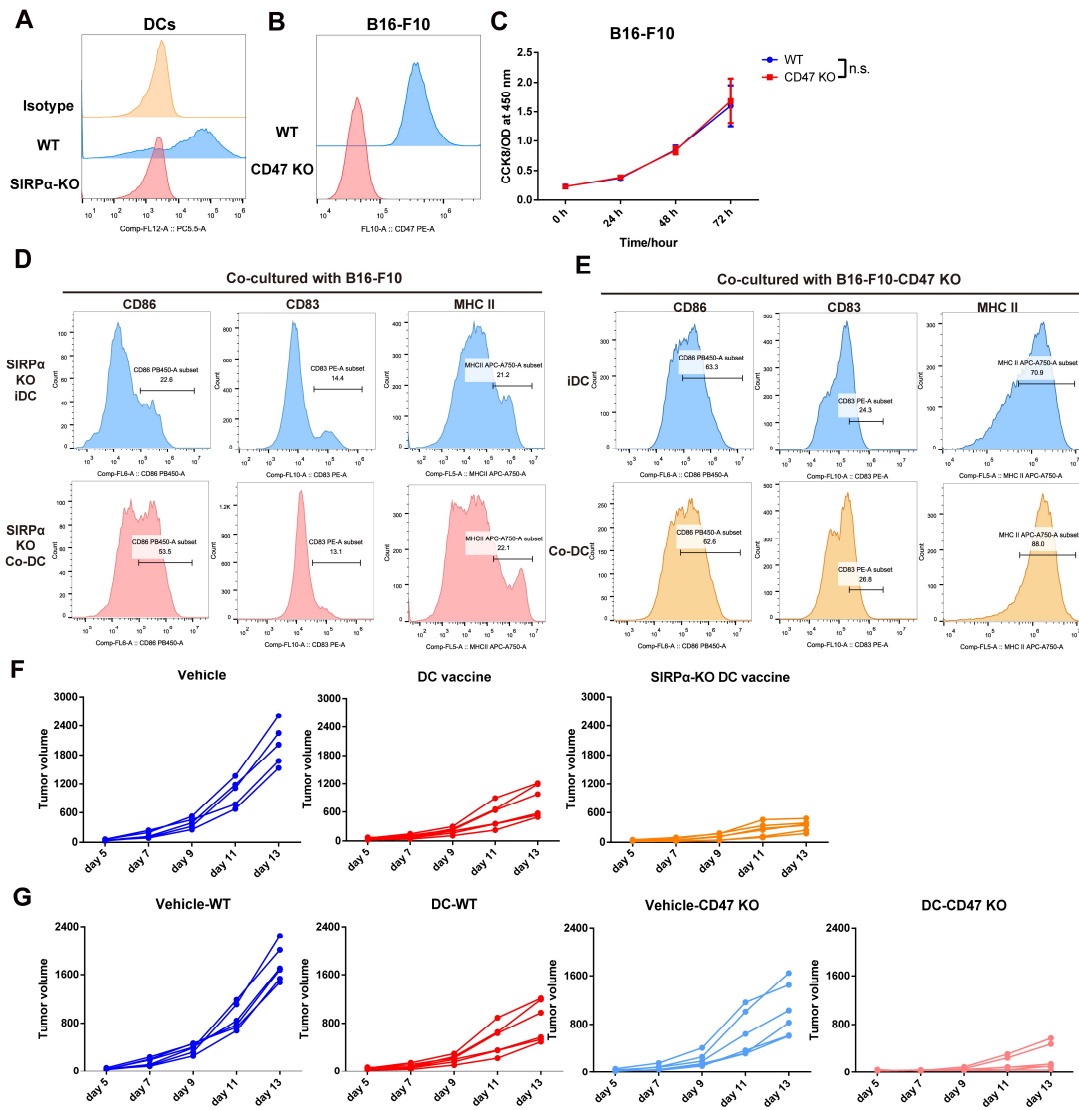


**Figure S4. SIRP $\alpha$ -CD47 knockout cancels the inhibition of DCs by tumor cells, related to Figure 5.**

A-B.) SIRP $\alpha$ -KO (A) or B16-F10-CD47 KO (B) verification.

C.) Growth curves of B16-F10-WT and B16-F10-CD47 KO tumor cells *in vitro*. Cell viability at every time point was evaluated by a CCK-8 assay. n=3. one-way ANOVA was used to determine the significance of differences between groups. Data are presented as the means  $\pm$  SDs.

D.) Representative histograms of CD86, CD83 and MHC II in SIRP $\alpha$ -KO DCs or WT-DCs after cocultured with B16-F10.

E.) The representative histograms of CD86, CD83 and MHC II expressed in untreated iDCs and Co-DCs cocultured with B16-F10-CD47 KO.

F-G.) Tumor growth curves for each mouse, as described in the experimental results

shown in Figure 3K (F) and Figure 3N (G), respectively. n=6 in every group.

*n.s.*, not significant; \* $p < 0.05$ ; \*\* $p < 0.01$ ; \*\*\* $p < 0.001$ .

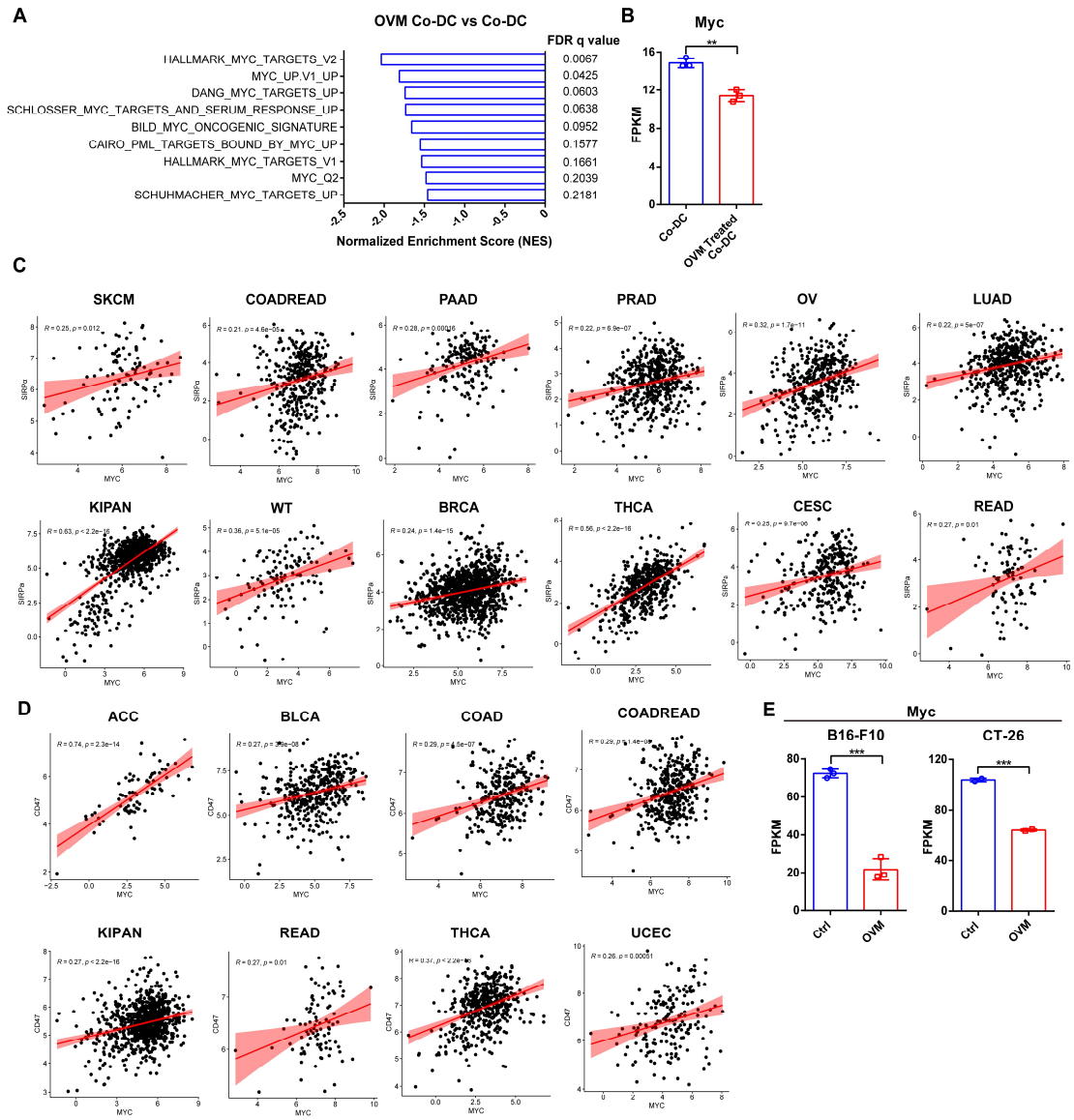


**Figure S5. MYC may be the potential transcription factor for OVM to regulate both SIRPα and CD47 expression, related to Figure 6.**

A.) Gene sets changes related to MYC regulation in OVM-treated Co-DCs compared to Co-DCs.

B.) Myc expression changes in B16-F10 cocultured Co-DCs and OVM-treated Co-DCs.

C-D.) Correlation analyses reveal associations between MYC and SIRPα expression (C), as well as between MYC and CD47 expression (D). SKCM: Skin Cutaneous Melanoma; COADREAD: Colon adenocarcinoma/Rectum adenocarcinoma Esophageal carcinoma; PAAD: Pancreatic adenocarcinoma; PRAD: Prostate adenocarcinoma; KIPAN: Pan-kidney cohort (including Kidney Chromophobe, Kidney renal clear cell carcinoma and Kidney renal

papillary cell carcinoma); WT: High-Risk Wilms Tumor; BRCA: Breast invasive carcinoma; THCA: Thyroid carcinoma; OV: Ovarian serous cystadenocarcinoma; LUAD: Lung adenocarcinoma; CESC: Cervical squamous cell carcinoma and endocervical adenocarcinoma; READ: Rectum adenocarcinoma. ACC: Adrenocortical carcinoma; BLCA: Bladder Urothelial Carcinoma; COAD: Colon adenocarcinoma; UCEC: Uterine Corpus Endometrial Carcinoma.

E.) Myc expression changes in OVM-infected B16-F10 (0.5 MOI) or CT-26 (1 MOI) tumor cells.

*n.s.*, not significant; \* $p < 0.05$ ; \*\* $p < 0.01$ ; \*\*\* $p < 0.001$ .

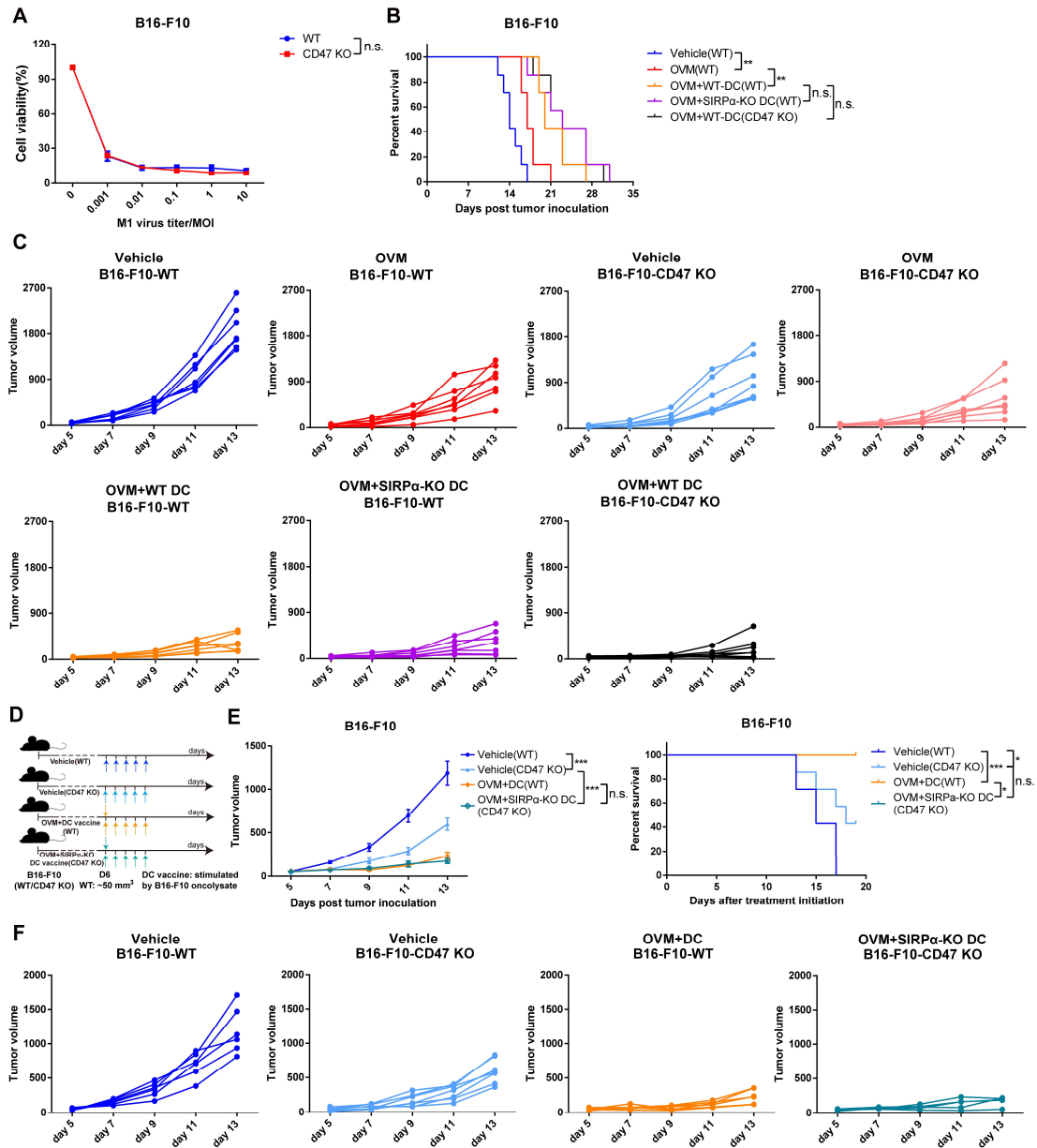


**Figure S6. OVM enhances the therapeutic effect of DC vaccine by blocking the interaction of SIRP $\alpha$ -CD47, related to Figure 6.**

A.) Cell viability assays were performed on B16-F10-WT and B16-F10-CD47 KO tumor cells 24 h after exposure to OVM.  $n=3$ . The data are shown as the means  $\pm$  SDs.

B-C.) The Kaplan–Meier survival curves (B) and tumor growth curves for each group (C) are linked to Figure 6I.  $p$  values were determined by the log-rank test.

D-F.) C57BL/6J mice were implanted subcutaneously in the right flank with B16-F10-WT or B16-F10-CD47 KO cells on day 0. On day 6, B16-F10-WT tumor-bearing C57BL/6J mice were treated with vehicle or OVM plus B16-F10 oncolysate-stimulated DC vaccine, and B16-F10-CD47 KO tumor-bearing C57BL/6J mice were treated vehicle or OVM plus

DC vaccine.

D.) Schematic diagram of the treatment regimen of B16-F10-WT and B16-F10-CD47 KO tumor-bearing C57BL/6J mice.  $n=6$ .

E.) Tumor growth curves and the Kaplan–Meier survival curves.  $p$  values were determined by one-way ANOVA at the final time point and the log-rank test, respectively.

F.) Tumor growth curves for each mouse in every group.

*n.s.*, not significant; \* $p < 0.05$ ; \*\* $p < 0.01$ ; \*\*\* $p < 0.001$ .

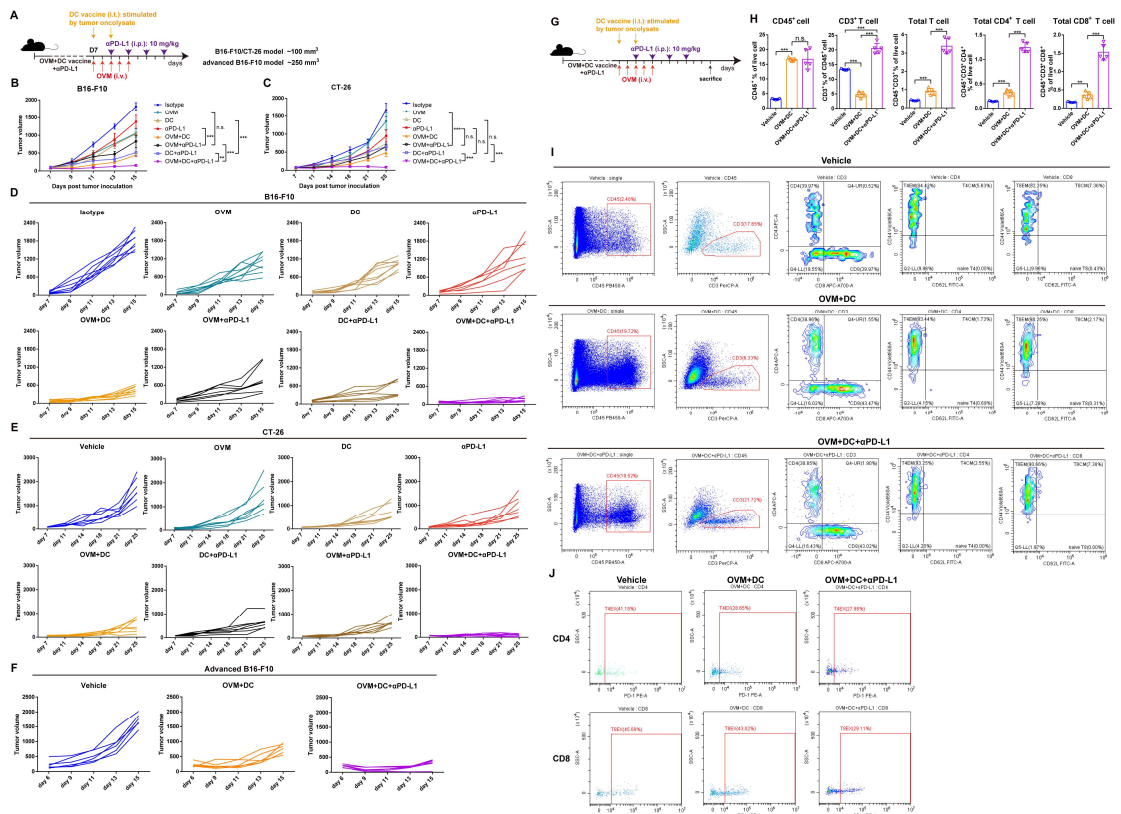


**Figure S7. PD-L1 blockade increases the efficacy of the combination of DC vaccine and OVM, related to Figure 7.**

A-F.) C57BL/6J or Balb/c mice were implanted subcutaneously in the right flank with B16-F10 or CT-26 cells on day 0 and treated with the indicated drugs.

A.) Schematic diagram of tumor inoculation and treatment in Figure 7D-F.

B-C.) Tumor growth curves in all groups are linked to Figure 7D (B) and E (C).

D-F.) Tumor growth curves for each mouse in every group derived from Figure 7D (D), E (E) and F (F).

G-J.) C57BL/6J mice were implanted subcutaneously in the right flank with B16-F10 cells and treated with corresponding therapy. Mice were sacrificed on the 3<sup>rd</sup> day after the last administration of αPD-L1 treatment, and infiltrated immune cells in the TME were analyzed by flow cytometry. n=5 in every group.

G.) Schematic diagram of the treatment regimen.

H.) The proportion of CD45<sup>+</sup> cells among live cells, CD3<sup>+</sup> T cells among CD45<sup>+</sup> cells, CD3<sup>+</sup> T cells among live cells, CD4<sup>+</sup> and CD8<sup>+</sup> T cells among live cells, respectively.

I.) Representative plot for the proportion of CD45, CD3, CD4, CD8, CD44 and CD62L,

respectively.

J.) Representative plot for the proportion of PD-1<sup>+</sup> among CD4<sup>+</sup> and CD8<sup>+</sup> T cells.

*p* values were determined by one-way ANOVA. *n.s.*, not significant; \**p* < 0.05; \*\**p* < 0.01;

\*\*\**p* < 0.001.